Novel Fabrication Technique for Three-Dimensional Micropatterned Electrospun Poly(DL-lactide-*co*-glycolide) Acid

Linus H. Leung, Hani Naguib

Department of Mechanical and Industrial Engineering, Department of Materials Science and Engineering, Institute of Biomaterials and Biomedical Engineering, University of Toronto, 5 King's College Road, Toronto M5S 3G8, Ontario, Canada

Received 29 April 2011; accepted 18 October 2011
DOI 10.1002/app.36385
Published online in Wiley Online Library (wileyonlinelibrary.com).

ABSTRACT: Current tissue engineering scaffolds created by electrospinning techniques are mostly limited to two-dimensional membranes. In this article, a novel method for fabricating three-dimensional (3D) fibrous scaffolds is presented. The fabrication technique uses the saturation of carbon dioxide in poly(lactide-*co*-glycolide) acid to lower the glass-transition temperature of the polymer to allow for the sintering of multiple layers of electrospun films. The effect of gas saturation on the films was first examined by variation of the saturation pressure and time. Fiber sintering was observed as the saturation pressure and time were increased. Next, the adhesion strength between two layers of scaffolds that were sintered by gas saturation was examined, and a higher pressure of 400 psi was found to better adhere the layers of the membranes together. From the first two parts of this study, the optimal combination of gas saturation parameters was determined to a pressure of 400 psi for 3 min. With this set of parameters, 3D structures were fabricated by the sintering of 30 layers of electrospun scaffolds. Also, by patterning individual layers using microfeatured plates, we improved the open porosity. This demonstration of the ability to fabricate 3D scaffolds improves current electrospinning techniques and maintains a desirable fibrous structure for tissue engineering. © 2012 Wiley Periodicals, Inc. J Appl Polym Sci 000: 000–000, 2012

Key words: biomaterials; mechanical properties; sintering

INTRODUCTION

Electrospinning is a technique that is widely used for fabricating scaffolds for tissue engineering. This process requires an electric field to apply electrostatic forces to draw nanosized to microsized fibers from an electrically charged polymer solution. The electrical field can be achieved by the attachment of electrodes of a high-voltage power supply to a polymer source and a collector plate to create the electrostatic force. The resulting scaffold is a membrane of random or aligned fibers. The high surface-area-to-volume ratio is favorable for cell adhesion.[1] The alignment of the fibers can also guide cell growth if needed.[2,3]

Scaffolds have been fabricated with this process on various polymers, including polycaprolactone,[4] collagen,[5] and poly(lactide-*co*-glycolide) acid (PLGA). Recently, nanocomposites have also been fabricated by the introduction of carbon nanotubes[6,7] or nanohydroxyapatite particles[8,9] in the polymer solution. The use of this technique with PLGA has also been reported extensively in the literature and has been shown to be suitable for tissue engineering applications.[8,10–12] PLGA, therefore, was also chosen for this study.

Different studies reported in the literature have been performed to examine the process parameters needed to control fiber morphology, and these processing parameters can be separated into three categories: solution properties, system settings, and environmental factors. The solution properties include the types and amounts of polymer and solvent used. Changing the material and solvent varies the viscosity and conductivity of the polymer solution, which can control the morphology of the scaffold from electrospraying beads to a beaded fiber structure or to a fiber-only structure.[10,13,14] The volatility of the solvent can also affect the fiber morphology because this property determines the solvent evaporation rate, which affects the solidification of the polymer fibers.[15] The system settings include the applied voltage, polymer solution feed rate, needle diameter, and collector distance. These settings can have correlated effects on the uniformity of the scaffold and the size of the fibers drawn.[16] Last,

Correspondence to: H. Naguib (naguib@mie.utoronto.ca).
Contract grant sponsors: Natural Sciences and Engineering Research Council of Canada, Canada Research Chairs Program, Canada Foundation of Innovation.

© 2012 Wiley Periodicals, Inc.

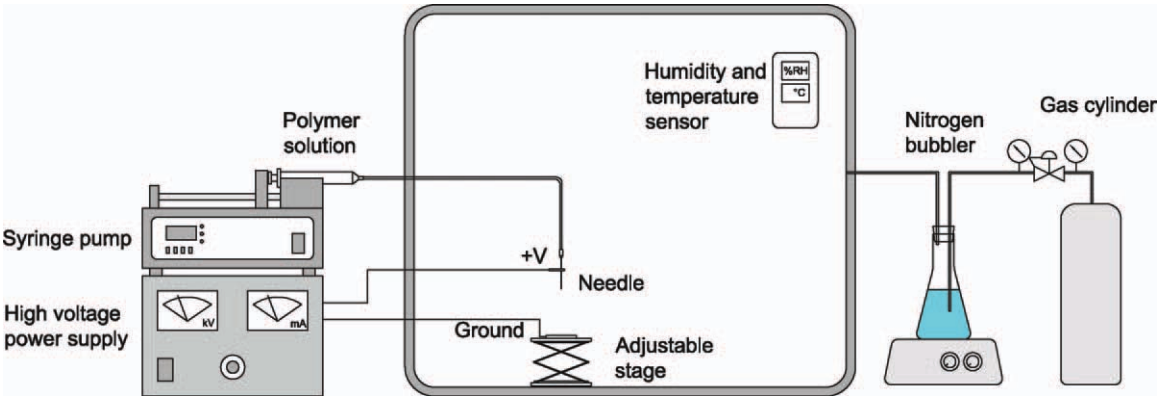

Figure 1 Illustration of the electrospinning setup. [Color figure can be viewed in the online issue, which is available at wileyonlinelibrary.com.]

the environmental factors, such as the temperature and humidity, can affect the evaporation of the solvent. A higher temperature and lower humidity encourage faster evaporation and can decrease the fiber size because the polymer may relax less than in a slower solvent evaporation.[17,18]

Work on controlling fiber morphology is abundant; however, the thickness of the membranes can still be restricted. This limitation is due to the electrically insulating properties of polymers. As a layer of polymer is deposited on the collector plate, the polymer insulates the collector, and the electric field can no longer be applied directly from the polymer source to the collector plate. Long deposition times of several hours can be used to increase the thickness to close to 2 mm, but this process is time-consuming. Building up a thick, three-dimensional (3D) scaffold can, therefore, be challenging, but it is desirable in some applications, such as bone tissue engineering, in which 3D structures may be necessary.

Researchers have been developing new techniques to fabricate 3D electrospun scaffolds. One technique uses dry ice at the collector such that ice crystals form on the membrane during electrospinning and act as a porogen.[19] The ice crystals then evaporate to leave a porous, fibrous structure. Another technique uses salt particles as the porogen. Salt particles are deposited onto the scaffolds after a film is first formed, and then, electropsinning is resumed such that new fibers are collected on the salt particles.[20] The salt is later leached out to leave a porous structure. In another study, chemical blowing agent particles were added, and the scaffolds were heated to evolve the gas from the blowing agent to form pores.[21] Other techniques use 3D collector designs such that the fibers form a 3D structure.[22,23]

In this article, a novel sintering technique for fabricating 3D electrospun scaffolds for bone tissue engineering is presented. This novel process combines two conventionally used techniques, gas foaming and electrospinning, to fabricate the scaffolds. The plasticizing effect of carbon dioxide (CO_2) on PLGA to lower the glass-transition temperature of the polymer has been documented,[24,25] and this effect was exploited to sinter layers of electrospun meshes together. When multiple layers were stacked during the gas saturation process, the layers adhered to form a 3D structure. Various combinations of gas saturation pressures and times were considered to determine an optimal set of parameters. In this study, the effect of the parameters on the single-layers scaffolds was first examined. Then, the quality of the adhesion between two layers was tested, and an optimal set of parameters was determined. Finally, with the optimal parameters, a 3D electrospun scaffold was fabricated.

EXPERIMENTAL

Experimental materials

Poly(DL-lactide-*co*-glycolide) acid (75/25 lactide/glycolide, SurModics Pharmaceuticals, Eden Prairie, MN) with a molecular weight of 113 kDa was used for this study. Reagent-grade acetone (Caledon Laboratories, Georgetown, Canada) was used as the solvent in the preparation of the polymer solution for electrospinning. Last, carbon dioxide was used for the sintering of the scaffolds.

Experimental setup

The electrospinning setup had several components and is illustrated in Figure 1. The positive (denoted as +V in the figure) and ground terminals of a high-voltage power supply by Gamma High Voltage Research were attached to the tip of a needle and a stainless steel collector, respectively. The terminals of a high-voltage power supply (Gamma High Voltage Research, Ormond Beach, FL), capable of supplying up to 30 kV, were attached to the tip of a needle and a stainless steel collector. A syringe pump was used to dispense the polymer solution.

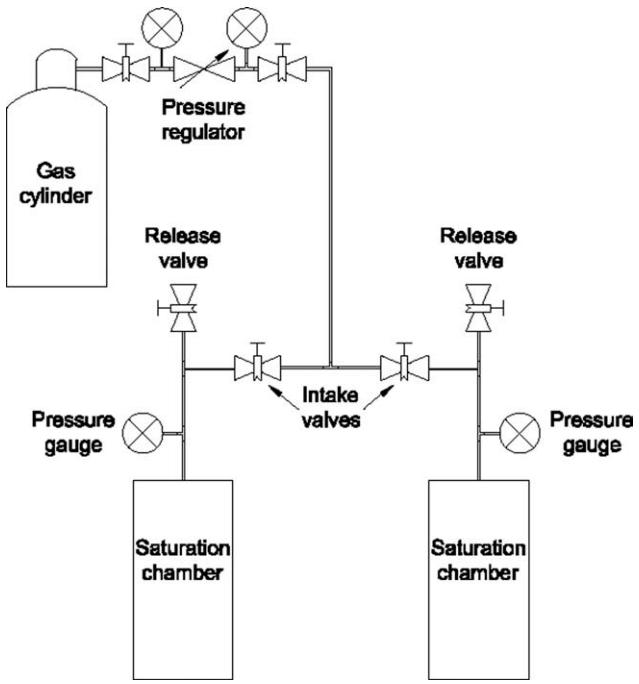

Figure 2 Schematic diagram of the batch-foaming setup.

Finally, nitrogen gas was used as a carrier gas for steam to maintain a constant humidity level in the electrospinning chamber. The temperature and relative humidity were monitored with a calibrated meter. A batch foaming setup, as illustrated in Figure 2, connected to a carbon dioxide cylinder was used for gas saturation.

Electrospinning technique

To perform the electrospinning experiments, a voltage of 20 kV was used, and the polymer solution was dispensed at a rate of 4.5 mL/h. A 20 wt % polymer solution was used, and the solution was stirred for 24 h to ensure that the polymer was completely dissolved. A 20-G (0.584-mm i.d.) needle was used, and the needle was cleaned with acetone after every run. The distance between the needle tip and the collector was kept at 15 cm. Last, a relative humidity of 50 ± 3% was maintained during electrospinning. These parameters were kept constant for this study and were chosen on the basis of the results of previous experiments, which showed that nonbeaded and consistent samples could be fabricated.[26] With these parameters, the scaffolds were electrospun for 2 min, and the electrospun films were cut into samples with a width and length of approximately 5 and 20 mm, respectively. A spinning time of 2 min was chosen, even though a higher spinning time could result in a thicker layer, because of the ease of fabrication and because the stacking of many layers could be more easily demonstrated.

Gas saturation technique

To identify the optimal saturation parameters for the adhesion of the samples, a parametric study was performed on the effects of pressure and saturation time. Three pressures, 200, 300, and 400 psi, were chosen, and saturation times of 1, 3, 5, 30, 60, and 120 min were used. Furthermore, the gas saturation was performed at room temperature. The gas saturation study was divided into three parts. The first was the study of the effect of gas saturation on the single-layer electrospun membranes. Second, the adhesion was characterized by the joining of two layers of the membranes together. As illustrated in Figure 3, two layers of the membranes were bonded together with a 0.5-mm spacer sandwiched between the two layers to keep one end of the rectangular samples from sintering such that these ends could be placed in the grips of the mechanical tester to measure the adhesion strength. A constant pressure of 0.35 kPa was applied on to the samples to keep the samples from deforming and distorting. Last, thick scaffolds were fabricated with the gas saturation parameters selected from the second part of this study by the sintering of 20–40 layers of electrospun meshes together. To fabricate a more porous scaffold, an additional patterning step was incorporated into the fabrication process. Before the stacking of the layers, each layer of the scaffold was individually pressed between two parallel serrated plates, as illustrated in Figure 4. The pyramids on the plates had base widths and heights of approximately 1 and 0.5 mm, respectively.

Scaffold characterization

The scaffolds were characterized for their change in morphology, density, and open porosity. To characterize the morphology of the scaffolds, fiber diameters were measured with image analysis software (ImageJ, U.S. National Institute of Health, Bethesda, MD) on micrographs taken with a scanning electron microscope. Over 25 fibers were measured at various locations of each sample, and this measurement served as an order of magnitude approximation to examine any changes in the fibers after the gas saturation process. The density was calculated through consideration of the mass and dimensions of the samples, and we calculated the relative density by taking the ratio of the scaffold density to the bulk density of

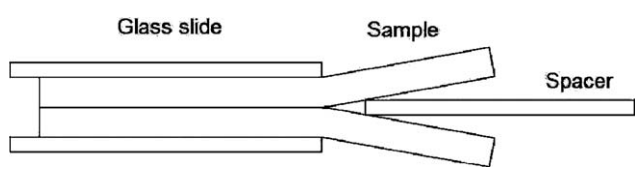

Figure 3 Setup for the adherence of two layers for the T-peel test.

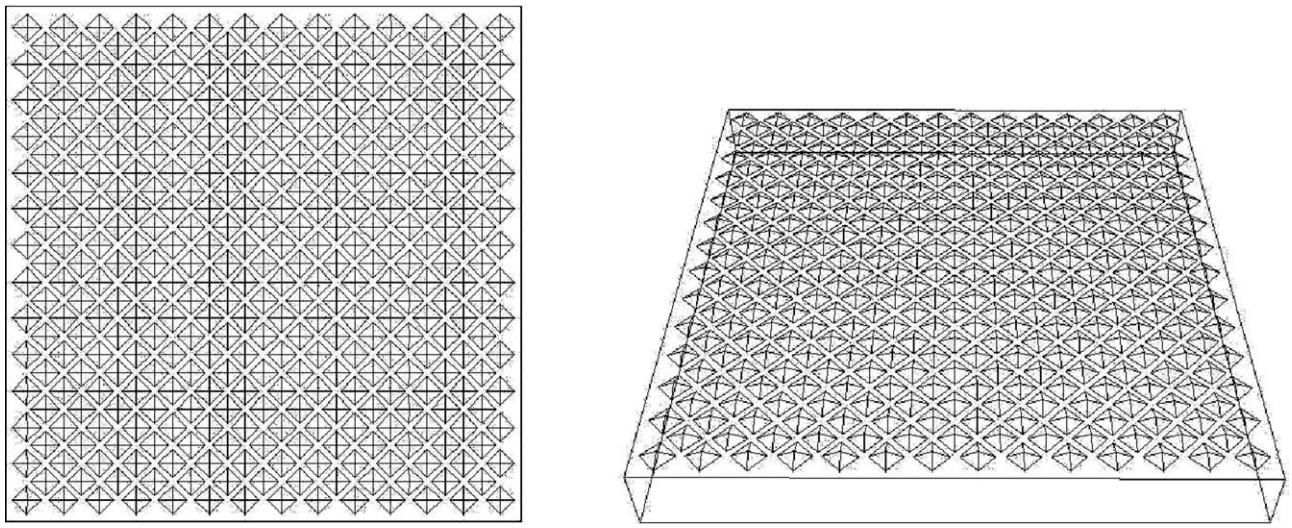

Figure 4 Diagram of the serrated press for patterning scaffold layers.

PLGA. Although the length and width of the samples were measured with calipers, we measured the thickness of the samples by viewing the cross sections of the samples under an optical microscope. Last, the open porosity was measured with a gas pycnometer (Quantachrome Ultrapycnometer 1000, Boynton Beach, FL). This equipment followed ASTM D 6226 to measure the volume of the sample that was closed to the environment (V_c), and the open porosity could then be calculated with eq. (1), where P is the open porosity and V_{scaff} is the geometric volume of the scaffold:

$$P = 1 - \frac{V_c}{V_{\text{scaff}}} \tag{1}$$

The single-layer membranes were tested in tensile mode at a crosshead speed of 1 mm/min with an Instron microtester (model 5848, Norwood, MA) equipped with a 50-N load cell. The width and length of the samples were approximately 0.5 and 2 cm, respectively. The modulus was taken as the slope of the initial linear region, and the 0.2% strain offset method was used to measure the yield strength of the samples.

The adhesion strengths of the samples were measured with a T-peel test on the basis of ASTM D 1867. The samples had lengths and widths of approximately 9 and 4 mm, respectively. The setup for this test is illustrated in Figure 5, and a testing speed of 1 mm/min was used. From the force and displacement data measured, the maximum adhesion strength (σ_{ad}) was calculated with eq. (2) and was defined as the maximum peeling force (F_{max}) over the width (w) of the sample:

$$\sigma_{\text{ad}} = \frac{F_{\text{max}}}{w} \tag{2}$$

The last mechanical test was performed on the thick, multilayered samples. These samples were tested in compression mode at 1 mm/min. The modulus and yield strength were found in a similar manner to the single-layer membranes, and all mechanical testing experiments were performed in triplicate.

RESULTS AND DISCUSSION

Electrospun scaffolds

The electrospun scaffolds were characterized for the pregas-saturated properties for comparison with the gas-saturated scaffolds. After 2 min of electrospinning,

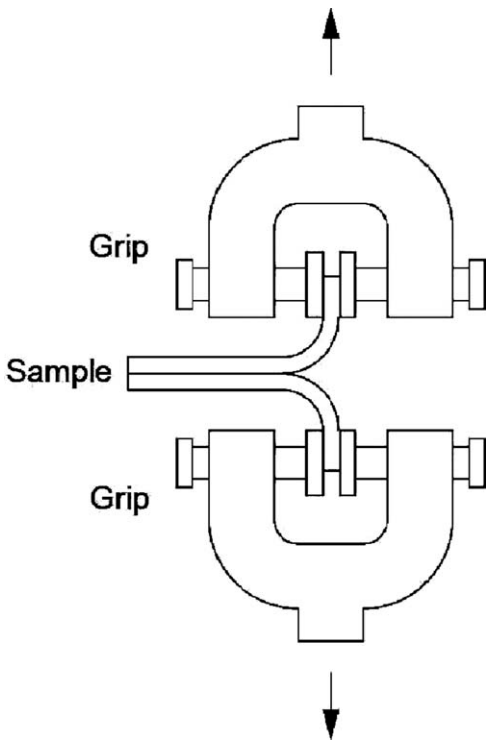

Figure 5 Setup for the T-peel test based on ASTM D 1867.

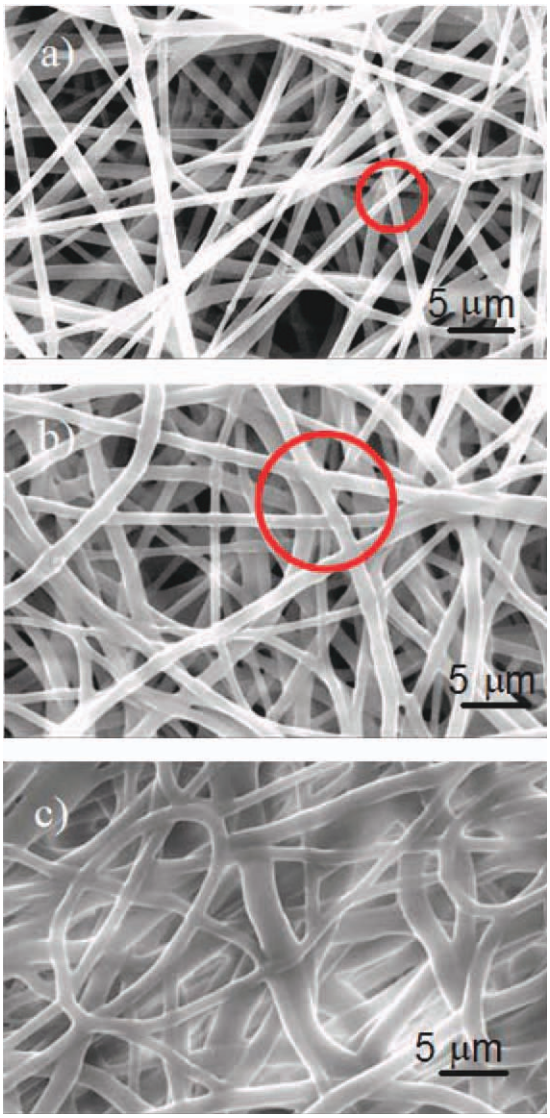

Figure 6 Micrographs of gas-saturated fibrous scaffolds showing (a) the unsintered structure at 200 psi for 5 min, (b) the sintered structure at 300 psi for 60 min, and (c) the densified fibrous structure at 400 psi for 5 min. [Color figure can be viewed in the online issue, which is available at wileyonlinelibrary.com.]

the thickness and fiber diameter of the scaffolds were approximately 98 ± 4 and 1.2 ± 0.2 μm, respectively. Also, the Young's modulus and yield strength of the preprocessed scaffolds were 220 ± 20 and 5.0 ± 0.4 MPa, respectively.

Effect of gas saturation on the single-layered scaffolds

The gas-saturated scaffolds were examined for changes in their morphologies. Figure 6 shows a collection of micrographs of the foamed scaffolds. At 200 psi, the fibers were not sintered together at any of the saturation times tested. At a higher pressure of 300 psi, short saturation times of 1 and 3 min did not cause the fibers to sinter; however, at 5 min, the fibers kept their individual shapes, but slight sintering could be seen. At 30 min, the fibers had fully sintered. Similar trends were observed for scaffolds pressurized at 400 psi, where some sintering occurred with 1 min of saturation, and the fibers merged with 3 min of saturation. At the highest tested saturation time for 400 psi, however, the fibrous structure was highly densified, and the spacing between fibers decreased. This structure is not desirable, as cells may not be able to proliferate into the scaffold.

The sintering of the fibers observed in the scaffolds processed at higher pressures and times was due to the plasticizing effect of carbon dioxide in PLGA. This plasticizing effect was measured by Yang et al.,[24] where the glass-transition temperature of PLGA was shown to decrease from approximately 43 to 31°C when the CO_2 pressure was increased to 400 psi. This temperature was near room temperature, and when the pressure was released, the gas molecules escaped the polymer matrix and further decreased the bonding between polymer chains to transition the polymer from the glassy state to the rubbery state such that the fibers in contact sintered together during the process.

The increases in the saturation pressure and time also affected the morphology of the fibers. As shown in the micrographs in Figure 6, the fiber appeared to be thicker and flatter. The first two micrographs showing the morphologies of samples saturated at 200 psi for 5 min and 300 psi for 60 min had average fiber diameters of 1.14 and 1.08 μm, respectively, whereas the sample processed at 400 psi for 5 min had an average diameter of 1.48 μm. The densifying and thickening of the fibrous structure may have been due to the excess amount of time allowed for

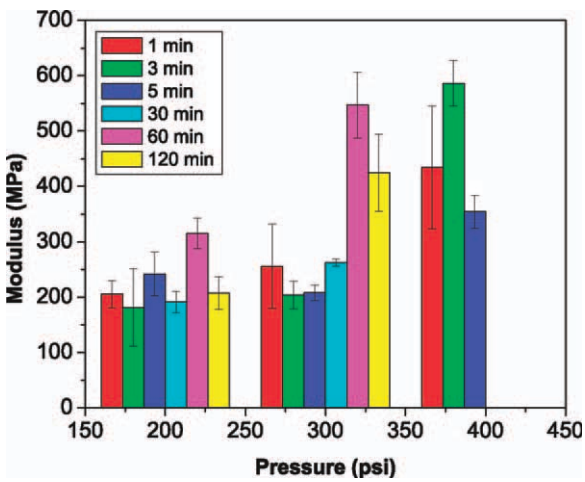

Figure 7 Young's modulus values of the gas-foamed scaffolds. [Color figure can be viewed in the online issue, which is available at wileyonlinelibrary.com.]

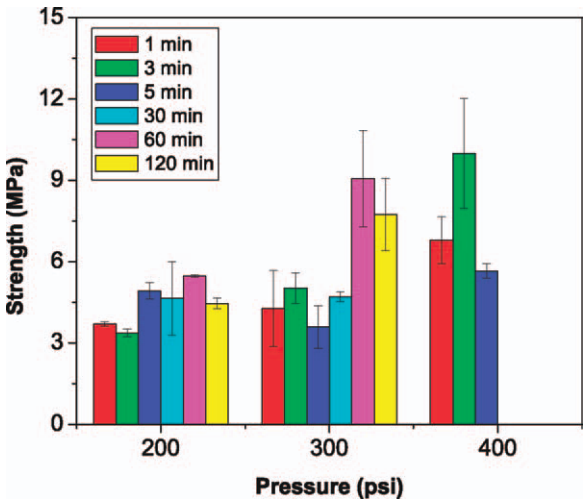

Figure 8 Yield strength of the gas-foamed scaffolds. [Color figure can be viewed in the online issue, which is available at wileyonlinelibrary.com.]

the relaxation of the polymer chains when the polymer chain mobility was increased in the high-pressure environment. Consequently, the fibers melted and increased in diameter. This phenomenon was also reported by Ayodeji et al.[27] in their study to examine the effect of carbon dioxide saturation in polycaprolactone.

The single-layer scaffolds were tested for their mechanical properties under tension, and the Young's modulus and yield strengths are presented in Figures 7 and 8, respectively. At 200 psi, the modulus and strength did not change; however, the gas saturation did affect the stress–strain behavior of the scaffolds; this is discussed further later. At 300 psi and short saturation times of up to 30 min, the mechanical properties did not deviate from the preprocessed scaffolds, in a similar manner as the samples saturated at 200 psi. When the saturation time was increased to 60 min, however, the modulus increased to 550 MPa, nearly 250% higher than in the preprocessed scaffolds. As shown in the micrographs, at 60 min of saturation, the fibers sintered together to provide a higher stiffness and strength to the scaffolds. Similarly, samples processed for 120 min showed improved mechanical properties. When a pressure of 400 psi was used, the modulus increased almost twofold, even when the samples were saturated for only 1 min because the fibers partially sintered. At 3 min, the modulus and strength further increased because of the higher degree of sintering of the fibers; however, at 5 min, the modulus decreased.

The stress–strain curves generated from the mechanical testing of samples processed at some of the saturation pressures and times are presented in Figure 9. The stress–strain curves for some processing parameters were omitted because of the similarity in behavior to the curves already shown. Examination of the curves of the unprocessed sample and the sample saturated at 200 psi for 5 min showed that although the modulus and strength of the two samples were similar, the elongation to break increased with gas saturation. Although the micrographs did not show a clear change in the morphology of the scaffolds, the higher extension may have been due to the relaxation of the polymer during gas saturation. When the polymer was electrospun, it was drawn into nanosized or microsized fibers from the spinneret, which was 0.58 mm in diameter. This large amount of drawing led to orientation of the polymer chains, which increased the tensile mechanical properties of the fibers. The orientation was lessened during the relaxation of the polymer chains when the glass-transition temperature was lowered during pressurization. Although sintering did not occur, the polymer chains may have been relaxed such that the fibers allowed for more elongation as the polymer chains aligned in the loading direction.

With further increases in the saturation pressure and time, the modulus, strength, and elongation at break all increased. This increase in the mechanical properties was due to the sintering of the fibers such that the resistance against the alignment of the fibers along the loading direction increased. The fracture of the samples also differed when we compared the sintered samples to the unprocessed and unaffected samples. Where the sintered samples fractured abruptly because of the ripping of the sample, the nonsintered samples tore apart slowly as the individual fibers broke such that the decrease in stress was more gradual.

As mentioned, the modulus and strength decreased when the scaffolds were saturated at 300 psi for 120 min and 400 psi for 5 min, although the

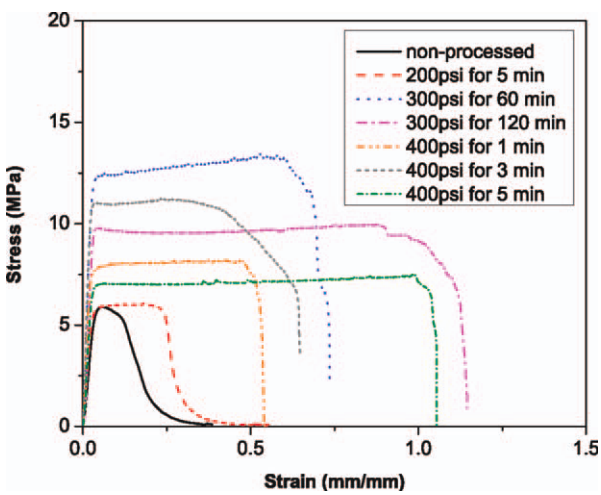

Figure 9 Stress–strain curves of processed, single-layer scaffolds. [Color figure can be viewed in the online issue, which is available at wileyonlinelibrary.com.]

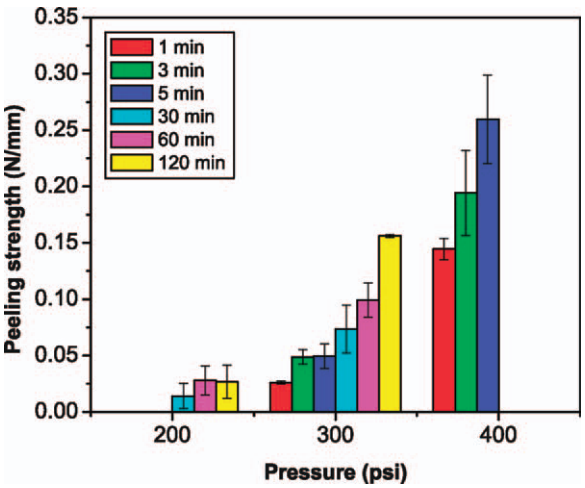

Figure 10 Adhesion strengths of the two layers of scaffolds. [Color figure can be viewed in the online issue, which is available at wileyonlinelibrary.com.]

elongation at break was over 100% strain. This decrease may have been due to the decrease of polymer chain alignment when the polymer was allowed to relax in the pressurized environment. This relaxation of the polymer chains may also have been the reason for the large elongation measured, as the fibers could have stretched more as the polymer chains aligned to the direction of load.

The decrease in mechanical properties may also have been due to the decrease in fiber density as the fiber diameter increased, as suggested by Li et al.[28] Under a tensile load, the randomly oriented fibers would resist reorientation but would eventually align to the direction of the load before fracture. A more densely packed mesh would have a higher resistance to the alignment of the fibers and, hence, would exhibit better mechanical properties. Although the quantification of the fiber density in the meshes was difficult because such a measurement can be subjective, the micrographs in Figure 6 show the decreased fiber density as the fibers relaxed and the increased diameter when the sample was saturated with 400 psi of carbon dioxide for 5 min.

From the perspective of maximizing the mechanical properties of the scaffolds for bone tissue engineering, saturating the samples at 400 psi for 3 min appeared to be the optimal set of parameters, as the fibers sintered together. To verify the sintering of the polymer, the adhesion strength was tested, and this is discussed in the next section.

Adhesion strength

The adhesion strength was determined by the layering of two samples together and by measurement of the maximum force required to peel the two layers apart. Figure 10 shows the maximum peeling strength recorded in the curves at all of the different processing parameters. The trend that the maximum adhesion strength increased with saturation time was apparent at all three pressures. The longer saturation times allowed more adhesion of the fibers between the two layers and increased the adhesion strength. Furthermore, as the pressure increased, the saturation strength also increased because of better sintering of the fibers. The best sintering strengths were achieved when the scaffolds were processed with 400 psi of pressure for 5 min; however, the use of this parameter led to the densification of the fibrous structure and was, therefore, undesirable. Pressures of 300 psi for 120 min and 400 psi for 3 min sintered the scaffolds similarly; therefore, to be more time-efficient, 400 psi for 3 min was selected to fabricate the 3D structures.

Noteworthy was that the peeling strength measured in this experiment may not have reflected the exact bonding strength between two layers of scaffolds. When the two layers were peeled, the samples may have strained and resisted the tensile load applied to them; therefore, the strength of each layer of the sample may have contributed to the overall adhesion strength that was measured and reported. For some samples, peaks in their peeling strength curves were observed either at the beginning or end of the experiment, as shown in the peeling strength curves of some specimens presented in Figure 11. These peaks may have been due to the stretching of the samples or to the larger force required to break the bonding between layers at the beginning or end points of adhesion. Upon closer examination of the force–displacement curves generated by the mechanical tester, the forces measured for the peeling of the two layers were usually less than 0.6 N, whereas the forces required to yield the single-layer scaffolds were always from 1 to 3 N. Because the forces

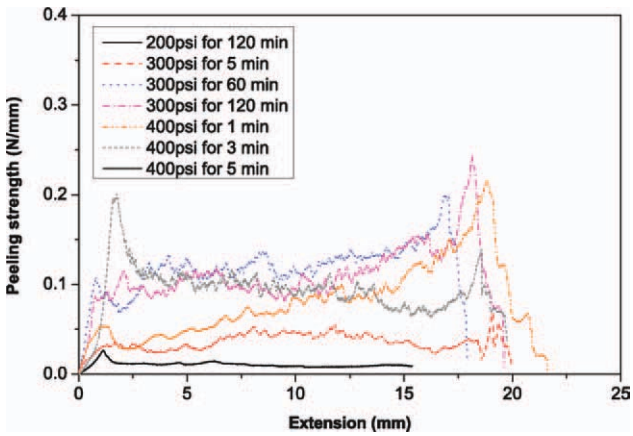

Figure 11 Peeling strength curves of the two layers of the sintered electrospun meshes. [Color figure can be viewed in the online issue, which is available at wileyonlinelibrary.com.]

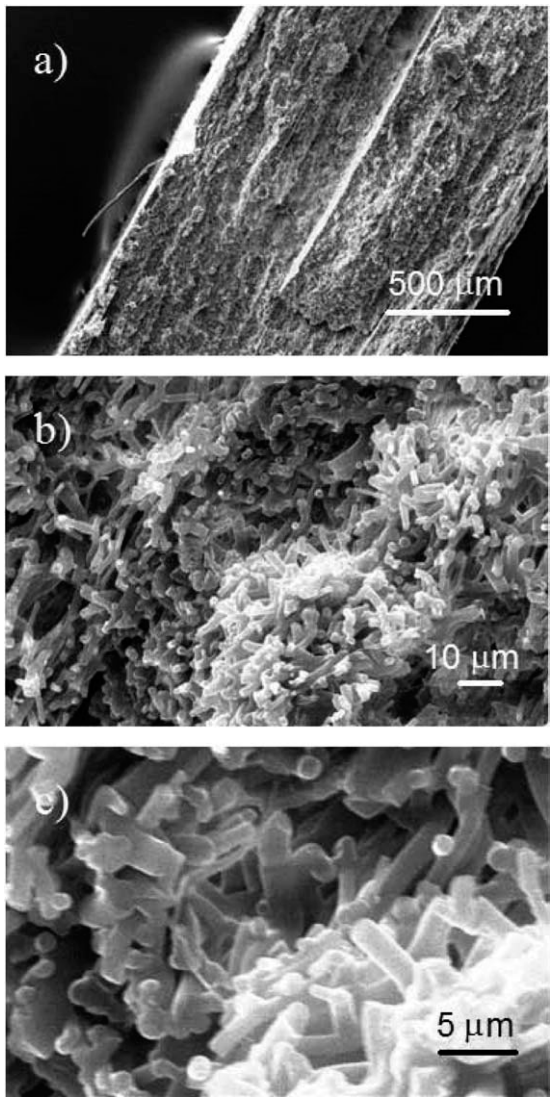

Figure 12 Micrographs of the cross section of the layered scaffolds at (a) 50, (b) 1000, and (c) 3000× magnifications.

required to yield the samples was higher than the peeling forces, the reported adhesion strength was assumed to be mostly due to the bonding that resisted the peeling of the two layers, and the rest was from the stretching of the individual layers.

Also worth mentioning is that the maximum peeling strength was reported, although these values usually occurred at the peaks. Lower peeling strengths were measured at the plateaus of the curves, and these values should better reflect the actual peeling strengths; however, these values were not reported because of the difficulty in taking the average value at the plateau. Nonetheless, the peeling strengths at the plateau followed similar trends as discussed for the maximum peeling strength, where the peeling strength increased with increasing gas saturation pressure and time. Furthermore, the adhesion strength values measured were used mainly as a criteria for selecting the sintering parameters for the 3D structure rather than an absolute characterization of the bond strength between layers. Because the plateau and peak values were similar for the higher saturation pressure and times, 400 psi for 3 min was selected.

3D scaffolds

In both sets of experiments of testing the mechanical properties of single-layer scaffolds and the adhesion of two scaffolds, the optimal set of processing parameter included a saturation pressure of 400 psi and a saturation time of 3 min. This set of parameters was, therefore, used to create 3D scaffolds. Twenty layers of the electrospun membranes were used to fabricate a scaffold that was approximately 1.4 mm in thickness. Figure 12 shows the micrographs of the cross section of a scaffold at different magnifications. As shown in the micrographs, the fibrous structure was preserved, and sintering of the fibers could be observed.

The fabricated samples had an average relative density of 0.511 ± 0.002 and an open porosity of 32 ± 9%. This open porosity was low for 3D scaffolds and may not have allowed the cells to grow into the center of the structure. Although the micrographs of the original scaffolds showed that open space was present between fibers, the meshes shrunk as the fibers relaxed, and the open space diminished. Mechanical testing was also performed on these 3D scaffolds in compression mode. From the stress–strain curves generated, the average Young's modulus and yield strength were found to be 31 ± 12 and 3.2 ±.2 MPa, respectively.

To fabricate a more porous scaffold to provide space for cells, an additional patterning step was incorporated into the fabrication process. Before the stacking of the layers, each layer of the scaffold was individually pressed between two parallel serrated plates, as illustrated in Figure 4, to form pyramidal microstructures, as shown in different magnifications in Figure 13. The plates created indentations with widths of approximately 500 μm. The goal was to use this structure to form pores inside the scaffold as the layers were stacked together. Thirty layers of the patterned meshes were then stacked and sintered with the process outlined previously to give a sample thickness of approximately 2.8 mm. The optimal saturation pressure of 400 psi for 3 min caused the flattening of the pyramidal structure because of excessive polymer relaxation; therefore, the saturation time was lowered to 1 min for fabrication of the patterned 3D structures. The micrograph of an edge of a patterned scaffold with 20 layers is presented in Figure 14. Also, the top layers were peeled off to examine the structure after the sintering process, and as shown in Figure 15,

the structure remained intact to form pores inside the scaffold.

The scaffolds were then characterized for their physical and mechanical properties. The relative density was measured to be 0.472 ± 0.002, which was nearly identical to the nonpatterned 3D scaffolds. The measured open porosity was 50 ± 1%, a 56% increase compared to the nonpatterned structures, and this increase improved the usability of the scaffolds. Although still low, the open porosity may be further enhanced through the use of other patterns, the puncturing of individual layers, or an increase in the interfiber spacing.[29]

The characterization of the mechanical properties of the scaffolds was examined next. These properties are important because the scaffold must be capable of withstanding the forces transferred from neighboring tissues, and it is also the medium that transfers the mechanical stimuli from the body to the bone cells. The compressive modulus and strength were measured to be 41.8 ± 0.7 and 3.98 ± 0.06 MPa, respectively. Although the open porosity increased by patterning the scaffolds, the density remained similar, and as a result, the mechanical properties did not degrade. The mechanical properties measured for these scaffolds were higher than for other highly porous polymeric scaffolds studied

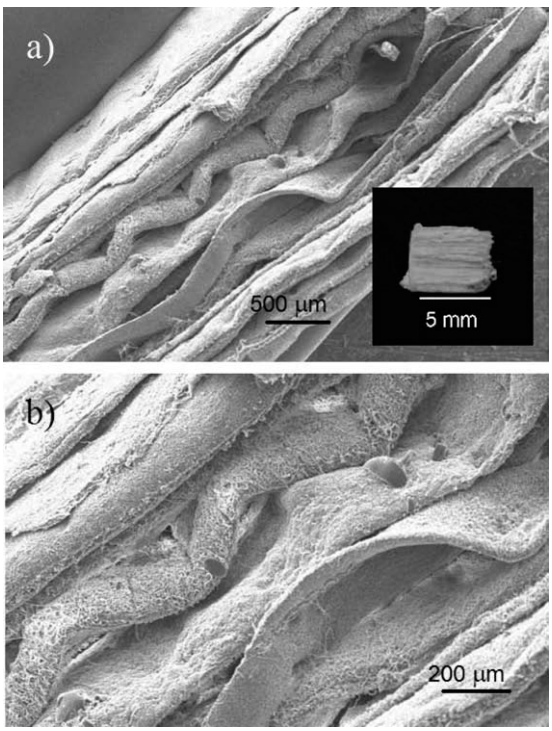

Figure 14 Micrographs of the patterned layers of the scaffolds at (a) 30× (with insert of a picture of a thick 3D scaffold fabricated with 40 layers) and (b) 70× magnifications.

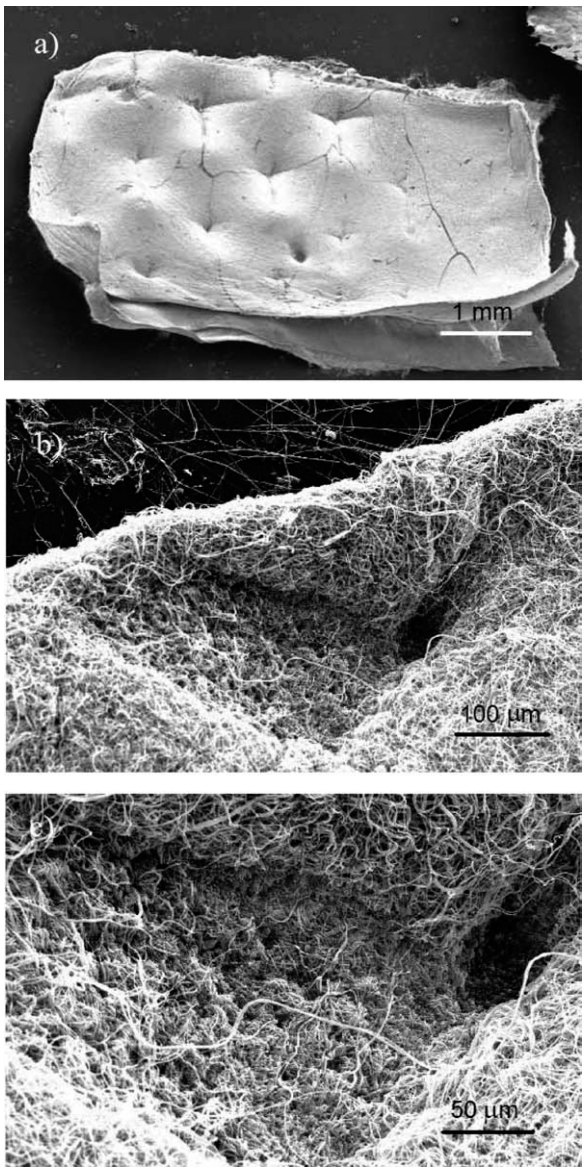

Figure 13 Layer of scaffold patterned with serrated plates at (a) 20, (b) 200, and (c) 400× magnifications.

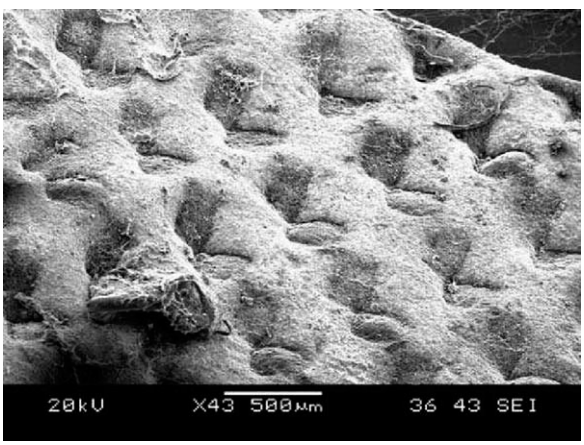

Figure 15 Structure remaining after the sintering process.

in the literature, for which a modulus of less than 10 MPa was usually obtained.[30–32] Although the higher properties showed improvements from typical porous polymeric scaffolds, the study of the local properties of the scaffolds, such as nanoindentation to examine the local stiffness, may be necessary in the future because these properties can affect cell differentiation, function, and growth.[33]

The number of layers was increased from 20 in the nonpatterned 3D scaffolds to 30 in the patterned scaffolds because a thickness of 1.4 mm was not higher than what has been shown in literature. To demonstrate the ability to further increase the thickness, a sample with 40 layers, shown in the insert of Figure 14(a), was fabricated, and a thickness of approximately 4.5 mm was measured. This showed that by increasing the number of layers, one can easily control the thickness of the samples.

CONCLUSIONS

The fabrication of 3D fibrous scaffolds was demonstrated in this study. The novel technique combines two conventionally used techniques, gas foaming and electrospinning. The use of CO_2 saturation lowered the glass-transition temperature of PLGA to allow for the sintering of the fibers. The first part of the study examined the effect of gas saturation on single-layer scaffolds, and the lowest pressure of 200 psi was ineffective in sintering the fibers. Similarly, a higher pressure of 300 psi at shorter saturation times of up to 30 min showed the same results. As the saturation time and pressure were increased, the fibers sintered to stiffen the scaffolds. In the two-layer adhesion test, the higher pressures produced better adhesion of the layers. For both parts of this study, a saturation pressure of 400 psi and a saturation time of 3 min were determined to be the optimal parameters, but the saturation time was lowered to 1 min for the micropatterning of individual layers. With this combination, micropatterned 3D scaffolds were successfully created. The pyramidal structure formed pores inside the 3D scaffold and increased the open porosity, and the thickness of the scaffolds could be controlled by variation of the number of layers used to fabricate the 3D samples. This novel technique improves on current scaffolds such that 3D fibrous structures can be fabricated. More important, more intricate designs may be patterned with this technique to form 3D structures.

References

1. Venugopal, J.; Zhang, Y. Z.; Ramakrishna, S. Proc Inst Mech Eng N J Nanoeng Nanosys 2004, 218, 35.
2. Xu, C. Y.; Inai, R.; Kotaki, M.; Ramakrishna, S. Biomaterials 2004, 25, 877.
3. Zhong, S.; Teo, W. E.; Zhu, X.; Beuerman, R. W.; Ramakrishna, S.; Yung, L. Y. L. J Biomed Mater Res A 2006, 79, 456.
4. Yoshimoto, H.; Shin, Y. M.; Terai, H.; Vacanti, J. P. Biomaterials 2003, 24, 2077.
5. Matthews, J. A.; Wnek, G. E.; Simpson, D. G.; Bowlin, G. L. Biomacromolecules 2002, 3, 232.
6. Zhang, H.; Chen, Z. J Bioact Compatible Polym 2010, 25, 241.
7. Saeed, K.; Park, S.; Lee, H.; Baek, J.; Huh, W. Polymer 2006, 47, 8019.
8. Jose, M. V.; Thomas, V.; Johnson, K. T.; Dean, D. R.; Nyairo, E. Acta Biomater 2009, 5, 305.
9. Bianco, A.; Di Federico, E.; Moscatelli, I.; Camaioni, A.; Armentano, I.; Campagnolo, L.; Dottori, M.; Kenny, J. M.; Siracusa, G.; Gusmano, G. Mater Sci Eng C 2009, 29, 2063.
10. You, Y.; Seung, J. L.; Byung, M. M.; Park, W. H. J Appl Polym Sci 2006, 99, 1214.
11. Li, W. J.; Laurencin, C. T.; Caterson, E. J.; Tuan, R. S.; Ko, F. K. J Biomed Mater Res 2002, 60, 613.
12. Ngiam, M.; Liao, S.; Patil, A. J.; Cheng, Z.; Chan, C. K.; Ramakrishna, S. Bone 2009, 45, 4.
13. Megelski, S.; Stephens, J. S.; Chase, D. B.; Rabolt, J. F. Macromolecules 2002, 35, 8456.
14. Tan, S. H.; Inai, R.; Kotaki, M.; Ramakrishna, S. Polymer 2005, 46, 6128.
15. Wannatong, L.; Sirivat, A.; Supaphol, P. Polym Int 2004, 53, 1851.
16. Zong, X.; Kim, K.; Fang, D.; Ran, S.; Hsiao, B. S.; Chu, B. Polymer 2002, 43, 4403.
17. Casper, C. L.; Stephens, J. S.; Tassi, N. G.; Chase, D. B.; Rabolt, J. F. Macromolecules 2004, 37, 573.
18. Medeiros, E. S.; Mattoso, L. H. C.; Offeman, R. D.; Wood, D. F.; Orts, W. J. Can J Chem 2008, 86, 590.
19. Simonet, M.; Schneider, O. D.; Neuenschwander, P.; Stark, W. J Polym Eng Sci 2007, 47, 2020.
20. Nam, J.; Huang, Y.; Agarwal, S.; Lannutti, J. Tissue Eng 2007, 13, 2249.
21. Kim, G.; Kim, W. J Biomed Mater Res B 2007, 81, 104.
22. Daming, Z.; Jiang, C. Nano Lett 2008, 8, 3283.
23. Zhang, K.; Wang, X.; Jing, D.; Yang, Y.; Zhu, M. Biomed Mater 2009, 4, 035004.
24. Yang, Y.; Zeng, C.; Lee, L. J. Adv Mater 2004, 16, 560.
25. Koushik, K.; Kompella, U. B. Pharm Res 2004, 21, 524.
26. Leung, L. H.; Hariri, S.; Naguib, H. E. In Proceedings of Biofoams 2009: 2nd International Conference on Biofoams, Niagra Falls, Toronto, Canada.
27. Ayodeji, O.; Graham, E.; Kniss, D.; Lannutti, J.; Tomasko, D. J Supercrit Fluids 2007, 41, 173.
28. Tuan, R. S.; Li, W.-J.; Cooper, J. A.; Mauck, R. L. Acta Biomater 2006, 2, 377.
29. Guimaires, A.; Martins, A.; Pinho, E. D.; Faria, S.; Reis, R. L.; Neves, N. M. Nanomed UK 2010, 5, 539.
30. Leung, L.; Chan, C.; Baek, S.; Naguib, H. Biomed Mater 2008, 3, 2.
31. Kim, S.; Ahn, K.; Park, M.; Lee, J.; Choi, C.; Kim, B. J Biomed Mater Res A 2007, 80, 206.
32. Kothapalli, C.; Shaw, M.; Wei, M. Acta Biomater 2005, 1, 653.
33. Chen, J.; Liu, C.; You, L.; Simmons, C. J Biomech 2010, 43, 108.